Potential of boron nitride/diamond heterostructure for n- and p-type conduction

Yao LI[1], Chenxu WANG[1], Qun LI[1,*], Jinfeng ZHANG[2], Kai SU[2], Jichao HU[1], Tao LIN[1], Zeyang REN[2], Jiaduo ZHU[2], Yachao ZHANG[2] and Yue HAO[2]

[1] *Department of Electronic Engineering, Xi'an University of Technology, Xi'an 710048, China;*

[2] *State Key Discipline Laboratory of Wide Band Gap Semiconductor Technology, School of Microelectronics, Xidian University, Xi'an 710071, China*

Appendix A

Following the model in Ref. [1], the hole density p_s in the BN/diamond heterostructure is deduced as

$$p_s = \frac{\varepsilon_0\varepsilon_b}{e^2 t_b}(E_g - \Phi_b + \Delta E_F - \Delta E_V) + N_A \frac{(t_b - t_i)^2}{2t_b} \tag{1}$$

where ε_b and ε_0 are the dielectric constants of BN barrier layer and the vacuum, t_b and t_i are the thicknesses of barrier layer and the undoped barrier layer. The term E_g is the energy band gap of BN barrier layer, Φ_b is the Schottky barrier height, ΔE_V is the valence band offset at the BN/diamond heterointerface, and N_A indicates the modulation doping density. Note that ΔE_F is the Fermi level with respect to the conduction band energy at the BN/diamond heterointerface and satisfies $\Delta E_F = E_0 + \left(\pi\hbar^2 / m_d^*\right)\cdot p_s$, where the ground state energy E_0 equals $\left[9\pi\hbar e^2 p_s \Big/ \left(8\varepsilon_0\varepsilon_s\sqrt{8m_d^*}\right)\right]^{2/3}$. Here, $\hbar$ is the reduced Planck constant, ε_s is the dielectric constant of the diamond, m_d^* is the density-of-state mass and equals $m_d^* = \left(m_{lh}^{*3/2} + m_{hh}^{*3/2} + m_{so}^{*3/2}\right)^{2/3}$ [2].

Appendix B

For the undoped barrier layer with thickness of 10, 20, and 50 nm, the dependence of hole density on the Schottky barrier height is shown in figure S1(a). The 2DHG density decreases with the increase of Schottky barrier height, and drops sharply when the Schottky barrier height exceeds 3.25 eV. For the presence of 2DHG, the Schottky barrier height Φ_b is no more than 3.58 eV for all considered barrier layer thickness. Lower Φ_b means weaker barrier depletion effect, and thus a higher 2DHG density can be expected. Figure S1(b) illustrates the variation of hole density with the thickness of undoped BN barrier layer for different Schottky barrier height. As implied in equation (1), the existence of 2DHG are only possible when $\Phi_b<(E_g-\Delta E_V)$, namely 3.59 eV. Consequently, it can be observed that when Φ_b equals 3.58 eV, the 2DHG density is

---

[*] Corresponding author (email: liqun@xaut.edu.cn)

already approaching the lower limit. While for a given Φ_b, the 2DHG density is inversely proportional to the barrier layer thickness. It is because that the decrease of barrier layer capacitance ($C_{tb}=\varepsilon_b\varepsilon_0/t_b$) with the barrier layer thickness would result in a diminishing 2DHG density, even the same voltage changes upon this capacitance.

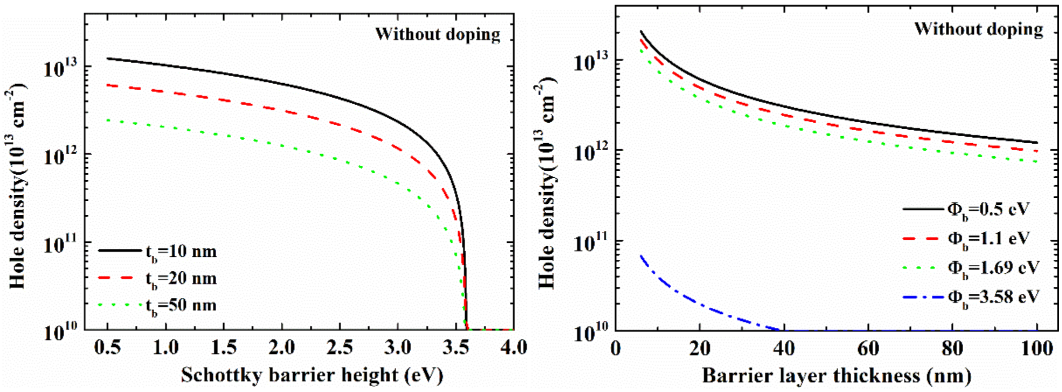

(a) (b)

Figure S1 (Color online) Variation of the hole density (a) with Schottky barrier height for different thickness of BN barrier layer of 10 nm, 20 nm and 50 nm without doping, (b) with barrier layer thickness for different Schottky barrier height of 0.5 eV, 1.1 eV, 1.69 eV and 3.58 eV without doping (b).

The 2DHG density is the resultant of both the terms related to the barrier layer capacitance and the doping effect, the former reduces the 2DHG density and the latter increases the 2DHG density with increasing barrier layer thickness. Figure S2 takes the uniformly doped barrier layer with the concentration of 1×10^{18} cm^{-3} as an example. The curves of 2DHG density versus t_b show totally different tendencies when $\Phi_b<3.58$ eV and when $\Phi_b\geq3.58$ eV. In the former case, the 2DHG density first descends (C_{tb} dominated) and then rises (N_A dominated) (e.g., Φ_b=0.5 eV). While for the latter case, the 2DHG density first rises sharply and then saturates due to its fully N_A dominated feature (e.g., Φ_b= 4.8 eV). The transit point at Φ_b of 3.58 eV is the very point where no doping, no 2DHG, but the exact point is N_A-dependent when N_A is available. For the highest Schottky barrier height of 4.8 eV, the hole is available only when the barrier is over 30 nm thick.

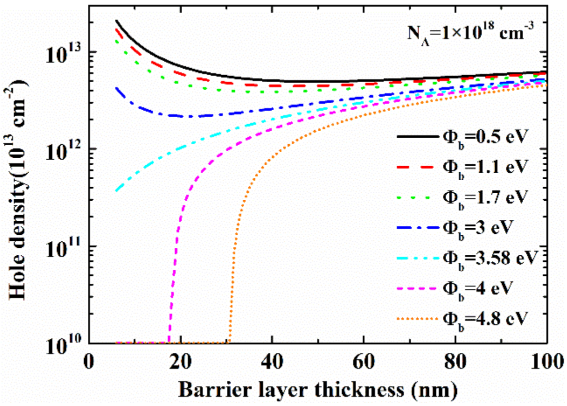

Figure S2 (Color online) Hole density versus BN barrier layer thickness with uniform doping of 1×10^{18} cm^{-3} under different Schottky barrier height.

Appendix C

The interface roughness (IFR) scattering is illustrated as [3]

$$\frac{1}{\tau}=\frac{\Delta^2 L^2 e^4 m_d^*}{2(\varepsilon_0\varepsilon_s)^2\hbar^3}\left(\frac{p_s}{2}\right)^2\int_0^1\frac{u^4\exp\left(-k_F^2L^2u^2\right)}{[u+G(q)q_{TF}/(2k_F)]^2\sqrt{1-u^2}}du, \qquad (2)$$

where Δ is the root mean square roughness height, L is the correlation length. The quantity e is the electron charge, $q_{TF}=m_d^*e^2/\left(2\pi\varepsilon_0\varepsilon_s\hbar^2\right)$ is the Thomas-Fermi screening wave vector, and $G(q)=1/8\left\{2[b/(b+q)]^3+3[b/(b+q)]^2+3[b/(b+q)]\right\}$ is a form factor, b is the variational parameter, $k_F=\sqrt{2\pi p_s}$ is the fermi-wave vector, and $u=q/(2k_F)$ is dimensionless with $q=2k_F\sin(\theta/2)$, $\theta\in(0,\pi)$.

The acoustic phonon (AC) scattering is illustrated as[3]

$$\frac{1}{\tau}=\frac{3m_d^*bk_BTD_{ac}^2}{16\rho u_l^2\hbar^3}, \qquad (3)$$

where k_B is the Boltzmann constant, D_{ac} is the acoustic deformation potential. The quantity ρ is the crystal mass density, and u_l is the velocity of longitudinal acoustic phonons.

The nonpolar optical phonon (NOP) scattering is illustrated as [3]

$$\frac{1}{\tau}=\int_{-\infty}^{\infty}|I|^2dq_z\cdot\frac{m_d^*D_{nop}^2}{4\pi\rho\hbar^2\omega_0}\left[N(\omega_0)+\frac{1}{2}\pm\frac{1}{2}\right]\times u\left(E(k)\mp\hbar\omega_0\right), \qquad (4)$$

where D_{nop} is the effective coupling constant covering, $|I|$ denotes the overlap integral and is shown as $|I|=\int_V\Psi_k^*\exp(iq\cdot r)\Psi_k dV$, $N(\omega_0)=1/\{\exp[\hbar\omega_0/(k_BT)]-1\}$ is the phonon occupation factor, $\hbar\omega_0$ is the phonon energy. The step function $u(x)$ satisfies $u(x\geq 0)=1$ and $u(x<0)=0$. The upper sign refers to the emission of a phonon by the carrier and the lower sign refers to the absorption of a phonon by the carrier.

The modulation doping (MD) scattering is illustrated as [4]

$$\frac{1}{\tau}=N_A\frac{m_d^*}{4\pi\hbar^3k_F^3}\left(\frac{e^2}{2\varepsilon_0\varepsilon_s}\right)^2\times\int_0^{2k_F}\frac{F(q)^2[\exp(-2qt_i)-\exp(-2qt_b)]q}{[q+q_{TF}G(q)]^2\sqrt{1-(q/(2k_F))^2}}dq, \qquad (5)$$

where $F(q)=\left[b/(b+q)\right]^3$ is the form factor of Fang-Howard wave function.

The remote surface roughness (RSR) scattering is illustrated as [5]

$$\frac{1}{\tau}=\frac{m_d^* N^2 e^4 {\Delta_R}^2 {L_R}^2}{8\hbar^3 \varepsilon_0^2 \bar{\varepsilon}^{-2}}\int_0^{2\pi}\left(1+\frac{1}{qt_b}\right)^2 \frac{\exp\left(-2qt_b-q^2{L_R}^2/4\right)}{\left[\varepsilon(q)\right]^2}\left(1-\cos\theta\right)P_0^2 d\theta, \tag{6}$$

where N is the average sheet density of the charges at barrier layer surface, and is assumed to be equal to the hole density in the BN/diamond interface. Δ_R and L_R are root mean square roughness height and correlation length at BN surface. $\bar{\varepsilon}$ is the average dielectric constant of the BN barrier and diamond layer, and $\varepsilon(q)$ is the dielectric constant accounting for the screening effect as

$$\varepsilon(q)=1+\frac{q_{TF}}{q}\left(G(q)+\frac{\varepsilon_s-\varepsilon_b}{\varepsilon_s+\varepsilon_b}F(q)^2\right). \tag{7}$$

Finally, the total carrier mobility is the sum of the contributions of the above five scattering mechanisms according to the Matthiessen's rule, $1/\mu_{total}=1/\mu_{RSR}+1/\mu_{IFR}+1/\mu_{AC}+1/\mu_{MD}+1/\mu_{NOP}$. Here, $\mu_i=e\tau_i/m_c^*$ is used to calculate each scattering mechanism limited mobility with τ_i the corresponding momentum relaxation time and m_c^* the conductivity mass ($m_c^*=\left({m_{lh}}^{*3/2}+{m_{hh}}^{*3/2}+m_{so}^{*3/2}\right)/\left({m_{lh}}^{*1/2}+{m_{hh}}^{*1/2}+m_{so}^{*1/2}\right)$) [6,7]. Here, the holes are assumed to be located only in the lowest subband, and the consideration of the multi-subband occupation and inter-subband scattering may result in a decreased hole mobility[8]. Parameters used in the calculation are listed in table S1.

Table S1 Parameters used in the calculation model.

Symbol	Quantity	Values
ε_b	Dielectric constant of BN	7.1 [9]
ε_s	Dielectric constant of diamond	5.7 [2]
E_g	Energy band gap of BN	5.67 [10]
m_{hh}^*	heavy hole mass	0.588m_0 [2]
m_{lh}^*	light hole mass	0.303m_0 [2]
m_{so}^*	spin-orbit hole mass	0.394m_0 [2]
ρ	Mass density	3515 kg/m^3
$\hbar\omega_0$	Phonon energy	165 meV
u_l	Velocity of longitudinal acoustic phonons	17536 m/s
ΔE_V	Valence band offset	2.08 eV [10]
D_{ac}	Acoustic deformation potential	8 eV [11]
D_{nop}	Effective coupling constant of the non-polar optical phonon	1.2×10^{10} eV/cm [11]
Δ	Root mean square roughness height for BN/diamond interface	1.2 nm [12]
L	Correlation length for BN/diamond interface	5 nm

Δ_R	Root mean square roughness height for BN surface	0.5 nm (~2MLs) [13]
L_R	Correlation length for BN surface	5 nm [13]

Appendix D

Figure S3 (a) shows that for the undoped BN barrier layer in VB1, the 2DHG mobility increases rapidly for BN barrier layer thinner than 5 nm, dominated by RSR and AC scattering, and saturates for larger barrier layer thickness, determined by AC scattering. The IFR and NOP scatterings matter only for thin BN barrier layer. The 2DHG mobility is 794 cm^2/Vs at room temperature for 20-nm-thick BN barrier layer. While for VB2 in figure S3 (b), the AC scattering is the only determining scattering mechanism in the considered thickness range of BN barrier layer. And the 2DHG mobility increases slightly with the increase of barrier layer thickness, whose value is generally larger than that in VB1. Specifically, the 2DHG mobility is 1572 cm^2/Vs in VB2 at room temperature for 20-nm-thick BN barrier layer, increased by almost two folds compared to VB1.

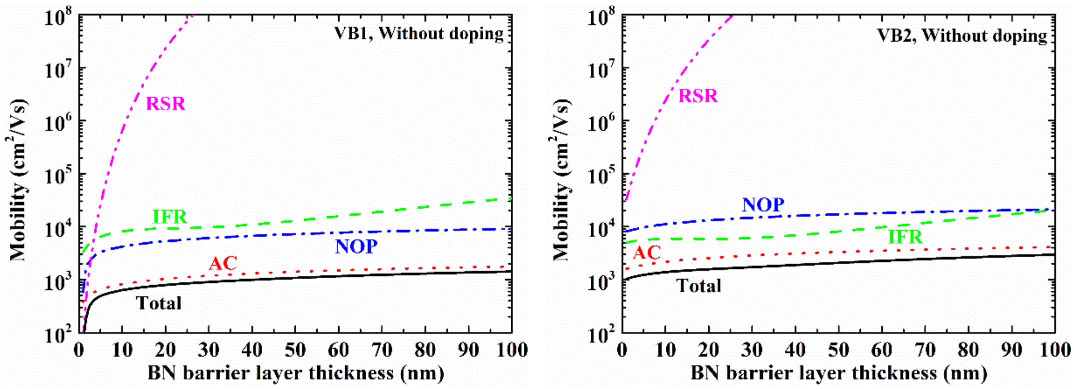

(a) (b)

Figure S3 (Color online) Mobility limited by different scattering mechanisms with the barrier layer thickness at room temperature without doping for VB1 (a) and VB2 (b).

While introducing the MD effect in the barrier layer in figure S4, the change in 2DHG mobility is minor due to the dominated AC scattering, whose values are within 528~731 cm^2/Vs and 1026~1408 cm^2/Vs for VB1 and VB2. The maximum mobilities for VB1 and VB2 locate at the similar barrier layer of 26 nm. The NOP scattering is the second important mechanism for VB1, while the IFR scattering ranks second for VB2. RSR scattering is more severe in VB2 and MD scattering is almost immune to the variation of *b*.

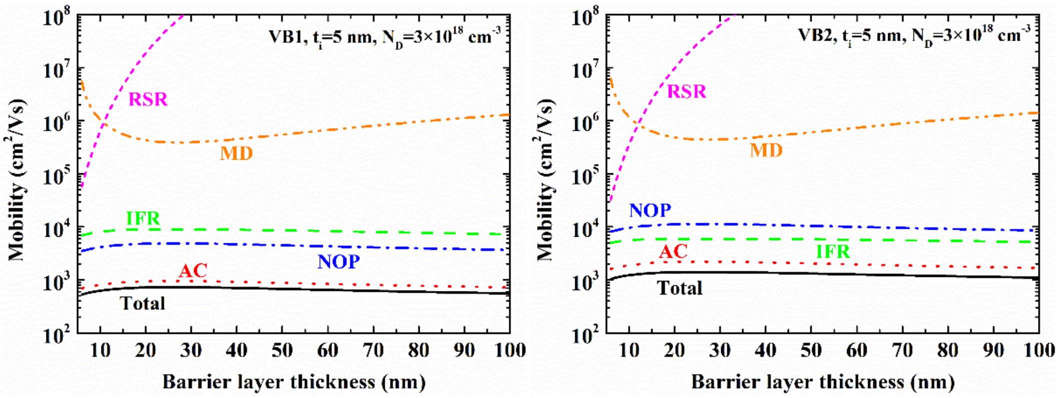

(a) (b)

Figure S4 (Color online) Mobility limited by different scattering mechanisms as the barrier layer thickness at room temperature with modulation doping for VB1 (a) and VB2 (b).

Then, the temperature-dependent mobilities for the heterostructure with undoped barrier layer are investigated in figures S5 (a) and (b). The thickness of BN barrier layer is chosen as 20 nm. In both cases, the IFR scattering is the strongest at low temperature, then AC scattering (VB1: 36~418 K, VB2: 129~420 K) and at last NOP scattering takes control for further increased temperature. Due to the weakened phonon scattering for VB2, the mobility at room temperature increases to 1506 cm^2/Vs, 1.9 times higher than that for VB1. While the mobility at low temperature is small in VB2 because of the strengthened IFR scattering.

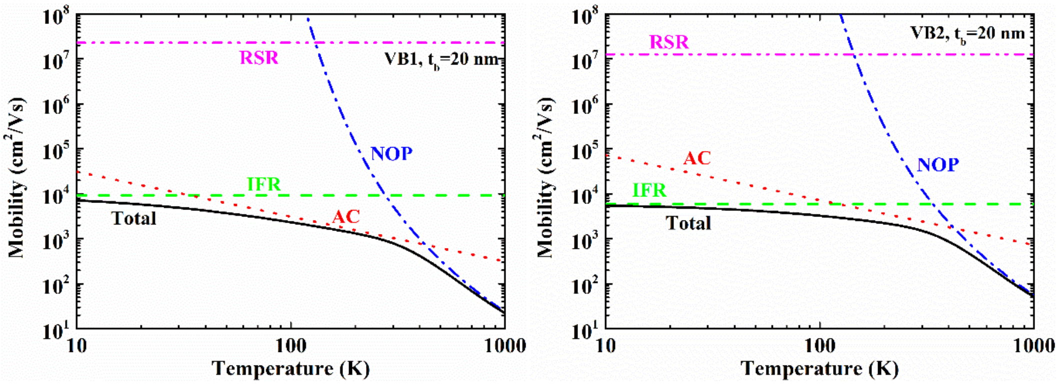

(a) (b)

Figure S5 (Color online) Temperature dependence of the mobility under different scattering mechanisms for the heterostructure consisting of a 20-nm-thick undoped BN barrier layer for VB1 (a) and VB2 (b).

The increased 2DHG density for the case with MD aggravates the IFR scattering from the heterointerface and the phonon scattering slightly. As shown in figure S6, the mobility reduction is not significant compared with the undoped case. Specifically, the mobilities at room temperature are 722 cm^2/Vs and 1395 cm^2/Vs for VB1 and VB2. Whereas, the RSR scattering and MD scattering in both cases are insignificant for the 2DHG mobility.

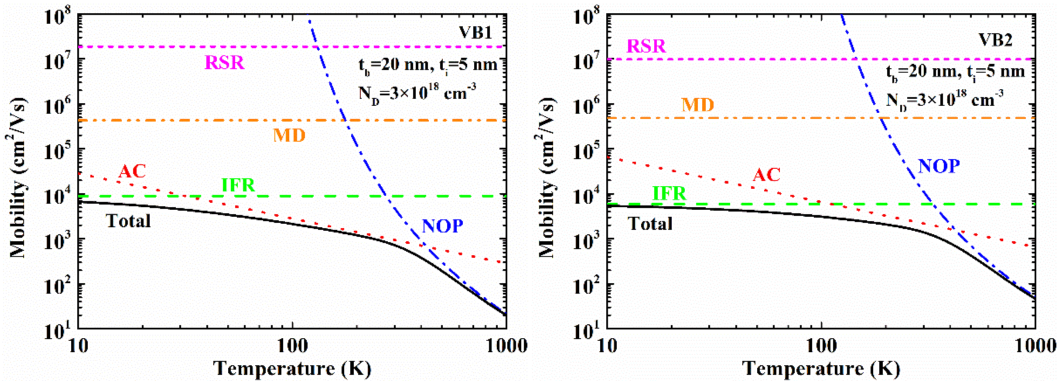

(a) (b)

Figure S6 (Color online) Temperature dependence of the mobility under different scattering mechanisms for the heterostructure consisting of a 20-nm-thick BN barrier layer with modulation doping for VB1 (a) and VB2 (b).

Appendix E

Then the contrasts are made for electron/hole mobility considering the difference in variational parameter *b*. Figure S7 shows the carrier mobility as a function of barrier layer thickness. The electron mobility curves follow the hole counterparts when the barrier is undoped or modulation doped in figure S7 (a), due to the similar key scattering mechanisms. That is, when the barrier thickness is less than 10 nm, the mobility of 2DEG and 2DHG of undoped structure is in the rising stage as a whole, while under modulation doping, the mobility of both decreases slowly. On the whole, the electron mobility is larger than hole mobility under the same barrier. Whereas, the hole mobility without barrier doping is over electron mobility with MD when barrier is thicker than 81 nm. The special barrier thickness is 55 nm for VB2 in figure S7 (b). The electron mobility is reduced in VB2 for thin and undoped barrier layer. After that, the mobility increments in VB2 are larger in electron than that in hole compared with VB1, indicating a more significant role that the parameter *b* plays in electron.

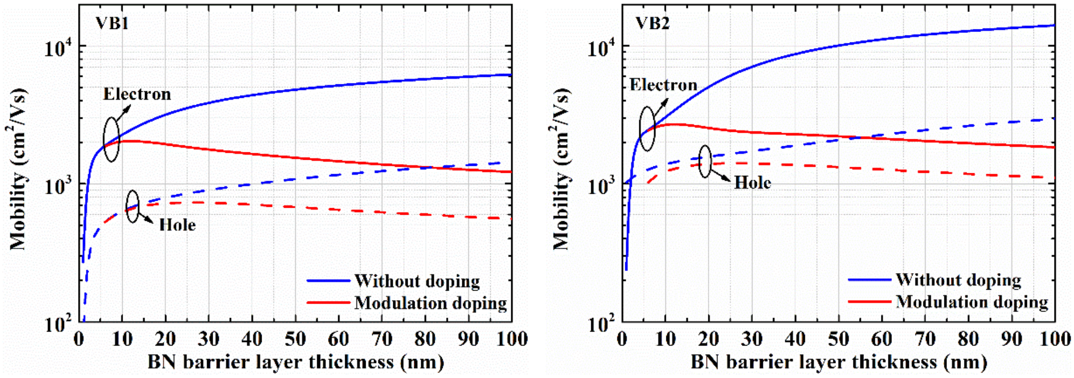

(a) (b)

Figure S7 (Color online) Comparison of electron and hole mobility as BN barrier layer thickness for the case without doping and with modulation doping for VB1 (a) and VB2 (b).

The changes of the mobility with temperature are studied for VB1 and VB2 in figure S8 (a) and figure S8 (b). With the increase of temperature, the mobilities first decrease slowly and then descend sharply when the temperature is over 300 K. The effect of MD on hole is minor in both cases, and is relatively large on electron, especially for the slowly-decreasing-mobility domain at low temperature. For VB2, both electron and hole mobilities are robust at high temperature, whereas the mobilities at low temperature are reduced compared with VB1, because of the strengthened IFR scattering.

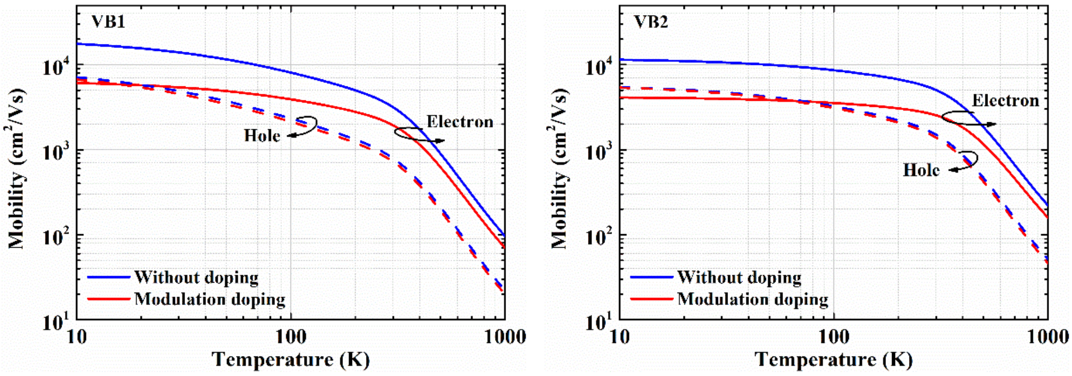

(a) (b)

Figure S8 (Color online) Comparison of electron and hole mobility as temperature for the case without doping and with modulation doping for VB1 (a) and VB2 (b).

References

[1] Delagebeaudeuf D, Linh N T. Metal-(n) AlGaAs-GaAs two-dimensional electron gas FET. IEEE Trans. Electron Devices, 1982, 29: 955-960

[2] Pernot J, Volpe P N, Omnès F, et al. Hall hole mobility in boron-doped homoepitaxial diamond. Phys. Rev. B 2010, 81: 205203

[3] Singh R, Stroscio A M, Dutta M. Phonon-Dominated Mobilities for Carriers in a Diamond Field Effect Transistor With a cBN Overlayer. IEEE Electron Device Lett., 2022, 43: 112-115

[4] Naka N, Fukai K, Handa Y, et al. Direct measurement via cyclotron resonance of the carrier effective masses in pristine diamond. Phys. Rev. B 2013, 88: 035205

[5] Li J, Ma T P. Scattering of silicon inversion layer electrons by metal/oxide interface roughness. J. Appl. Phys., 1987, 62: 4212-4215

[6] Tsukioka K. Scattering Mechanisms of Carriers in Natural Diamond. Jpn. J. Appl. Phys., 2001, 40: 3108-3113

[7] Tsukioka K, Okushi H. Hall Mobility and Scattering Mechanism of Holes in Boron-Doped Homoepitaxial Chemical Vapor Deposition Diamond Thin Films. Jpn. J. Appl. Phys., 2006, 45: 8571-8577

[8] Li Q, Li Y, Zhang Y et al. Multi-Subband Polar Optical Phonon Scattering in InAlN/AlN/GaN Heterostructures. Phys. Status Solidi RRL, 2023: 2300238

[9] Chilleri J, Wang Y N, Shur M S, et al. A low-field electron mobility analysis of cubic boron nitride. Solid State Commun., 2022, 352: 114776

[10] Chen J R, Tao R, Wang G, et al. The interface microstructure and band alignment of hexagonal boron nitride/diamond heterojunctions. J. Mater. Chem. C, 2023, 11: 5324

[11] Li Y, Zhang J F, Liu G P, et al. Mobility of Two-Dimensional Hole Gas in H-Terminated Diamond. Phys. Status Solidi RRL, 2018, 12: 1700401

[12] Peterson R, Malakoutian M, Xu X Q, et al. Analysis of mobility-limiting mechanisms of the two-dimensional hole gas on hydrogen-terminated diamond. Phys. Rev. B 2020, 102: 075303

[13] Cao Y, Xing H L, Jena D. Polarization-mediated remote surface roughness scattering in ultrathin barrier GaN high-electron mobility transistors. Appl. Phys. Lett., 2010, 97: 222116